ENVIRONMENTAL RESEARCH
CLIMATE

ACCEPTED MANUSCRIPT • OPEN ACCESS

Mid-latitude clouds contribute to Arctic amplification via interactions with other climate feedbacks

To cite this article before publication: David B Bonan *et al* 2025 *Environ. Res.: Climate* in press https://doi.org/10.1088/2752-5295/ada84b

Mid-latitude clouds contribute to Arctic amplification via interactions with other climate feedbacks

David B. Bonan
Environmental Science and Engineering, California Institute of Technology, Pasadena, CA
E-mail: dbonan@caltech.edu

Jennifer E. Kay
Department of Atmospheric and Oceanic Sciences, University of Colorado, Boulder, CO
Cooperative Institute for Research in Environmental Sciences, University of Colorado, Boulder, CO

Nicole Feldl
Department of Earth and Planetary Sciences, University of California Santa Cruz, Santa Cruz, CA

Mark D. Zelinka
Lawrence Livermore National Laboratory, Livermore, CA

Abstract. Traditional feedback analyses, which assume that individual climate feedback mechanisms act independently and add linearly, suggest that clouds do not contribute to Arctic amplification. However, feedback locking experiments, in which the cloud feedback is disabled, suggest that clouds, particularly outside of the Arctic, do contribute to Arctic amplification. Here, we reconcile these two perspectives by introducing a framework that quantifies the interactions between radiative feedbacks, radiative forcing, ocean heat uptake, and atmospheric heat transport. We show that including the cloud feedback in a comprehensive climate model can result in Arctic amplification because of interactions with other radiative feedbacks. The surface temperature change associated with including the cloud feedback is amplified in the Arctic by the surface-albedo, Planck, and lapse-rate feedbacks. A moist energy balance model with a locked cloud feedback exhibits similar behavior as the comprehensive climate model with a disabled cloud feedback and further indicates that the mid-latitude cloud feedback contributes to Arctic amplification via feedback interactions. Feedback locking in the moist energy balance model also suggests that the mid-latitude cloud feedback contributes substantially to the intermodel spread in Arctic amplification across comprehensive climate models. These results imply that constraining the mid-latitude cloud feedback will greatly reduce the intermodel spread in Arctic amplification. Furthermore, these results highlight a previously unrecognized non-local pathway for Arctic amplification.

Keywords: Arctic amplification, cloud feedbacks, climate change, climate models

Submitted to: *Environ. Res.: Climate.*

1. Introduction

The Arctic warms more than the global average in response to increased greenhouse gas concentrations. This phenomenon, referred to as 'Arctic amplification', has been a robust feature of climate change simulations for several decades (Manabe and Wetherald, 1975; Manabe and Stouffer, 1980; Holland and Bitz, 2003) and has recently become evident in observations (Polyakov et al., 2002; Serreze et al., 2009; England et al., 2021). Arctic amplification has been attributed to numerous processes, including sea ice changes (Manabe and Wetherald, 1975; Holland and Bitz, 2003; Winton, 2006; Graversen and Wang, 2009; Feldl and Merlis, 2021), increased poleward energy transport (Holland and Bitz, 2003; Hwang et al., 2011; Singh et al., 2017; Merlis and Henry, 2018; Beer et al., 2020), local radiative forcing and raditive feedbacks (Pithan and Mauritsen, 2014; Payne et al., 2015; Stuecker et al., 2018; Henry et al., 2021; Hahn et al., 2021), and interactions between poleward energy transport and radiative feedbacks (Bonan et al., 2018; Russotto and Ackerman, 2018; Russotto and Biasutti, 2020; Feldl et al., 2020; Beer and Eisenman, 2022; Chung and Feldl, 2024; England and Feldl, 2024). However, despite extensive research on the mechanisms of Arctic amplification, contemporary climate models continue to show considerable spread in its magnitude under greenhouse-gas forcing (Feldl et al., 2020; Hahn et al., 2021).

The factors contributing to Arctic amplification are typically quantified by examining changes in the local atmospheric energy budget under warming (Crook et al., 2011; Pithan and Mauritsen, 2014; Feldl et al., 2017; Goosse et al., 2018; Hahn et al., 2021). This method, which we hereafter refer to as the 'traditional feedback-forcing framework', attributes the change in surface temperature (ΔT) to partial temperature contributions from radiative forcing ($\mathcal{F}$), radiative feedbacks (λ), ocean heat uptake (ΔG), and the change in atmospheric heat transport ($\Delta\left(\nabla \cdot F\right)$) via

$$\Delta T = \frac{1}{\lambda_0}\Bigg(- \mathcal{F} - \lambda \Delta T + \Delta G + \Delta(\nabla \cdot F) - \epsilon \Bigg), \quad (1)$$

where λ_0 is the global- and annual-mean Planck feedback, and the net radiative feedback is

$$\lambda = \sum_{i \neq 0} \lambda_i, \quad (2)$$

where i denotes an individual radiative feedback (e.g., surface-albedo feedback) and the Planck feedback at regional scales is represented by deviations from λ_0. Note that ϵ is a residual term and usually quite small (Caldwell et al., 2016; Zelinka et al., 2020; Hahn et al., 2021).

The traditional feedback-forcing framework has been powerful in understanding the magnitude, seasonality, and intermodel spread of Arctic amplification across climate models (e.g., Pithan and Mauritsen, 2014; Hahn et al., 2021). For example, applying this framework to a simulation in which atmospheric carbon dioxide concentrations are abruptly doubled in CESM1-CAM5—a widely used comprehensive climate model (Hurrell et al., 2013)—reveals that the Arctic (60°N–90°N) warms 3.1× more than the Tropics (30°S–30°N) due to the surface-albedo, Planck, and lapse-rate feedbacks (Fig. 1a), consistent with previous studies (Pithan and Mauritsen, 2014; Previdi et al., 2020; Hahn et al., 2021). This decomposition, applied to CESM1-CAM5 and other climate models participating in Phase 5 and 6 of the Coupled Model Intercomparison Project (CMIP5 and CMIP6; Taylor et al., 2012; Eyring et al., 2016), indicates that the cloud feedback does not contribute to warming in the Arctic (Fig 1a; Pithan and Mauritsen, 2014; Previdi et al., 2020; Hahn et al., 2021).

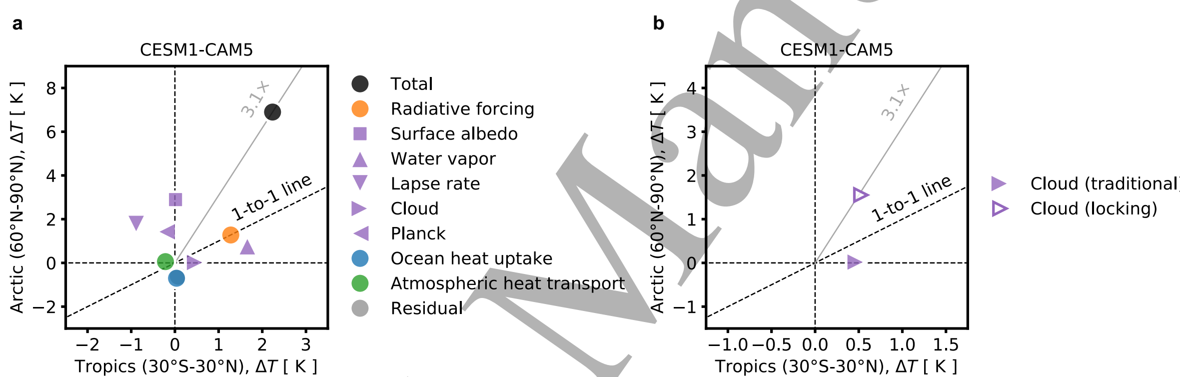

Figure 1. Contributions to Arctic amplification in CESM1-CAM5. (a) Contributions to surface temperature change in the (x-axis) Tropics (30°S-30°N) and (y-axis) Arctic (60°N-90°N) for years 100–150 of a CESM1-CAM5 abrupt-2xCO2 simulation. The black dot denotes the total surface temperature change and each colored symbol denotes a specific mechanism in Eq. (1). The colored symbols sum to the black dot. (b) Contribution of the cloud feedback to surface temperature change in the (x-axis) Tropics (30°S-30°N) and (y-axis) Arctic (60°N-90°N) for a CESM1-CAM5 abrupt-2xCO2 simulation diagnosed from the traditional feedback-forcing perspective (purple triangle) and diagnosed from the feedback locking perspective (white triangle). The grey lines and numbers indicate the magnitude of Arctic amplification.

While the traditional feedback-forcing framework can explain climate model behavior under greenhouse gas forcing, it assumes feedback mechanisms act independently and add linearly, which hinders our mechanistic understanding of surface temperature change. Studies have addressed this limitation by conducting feedback locking experiments (Wetherald and Manabe, 1988; Hall, 2004; Vavrus, 2004; Graversen and Wang, 2009; Langen et al., 2012; Mauritsen et al., 2013; Merlis, 2014; Voigt et al., 2019; Middlemas et al., 2020; Chalmers et al., 2022), in which the radiative effect of a physical process, such as water vapor or clouds, is disabled, and its impact on climate is examined in simulations both with and without the process. For example, Middlemas et al. (2020) and Chalmers et al. (2022) showed that when the cloud feedback is disabled in the same greenhouse-gas forcing CESM1-CAM5 simulation as above, the magnitude of warming is substantially reduced across the globe. In this approach, the effect of the cloud feedback on surface temperature change can be quantified as the difference between the greenhouse-gas forcing simulation where the cloud feedback is active, and the greenhouse-gas forcing simulation where the cloud feedback is inactive. This perspective suggests that the cloud feedback contributes to approximately 0.5 K of warming in the Tropics and 1.5 K of warming in the Arctic (right white triangle, Fig. 1b). This directly contradicts the traditional feedback-forcing perspective, which suggests the cloud feedback does not contribute to Arctic warming (right purple triangle, Fig. 1b). In fact, warming is still 3.1× larger in the Arctic when compared to the Tropics (grey line, Fig. 1b), indicating that the cloud feedback contributes to Arctic amplification when quantified from the feedback locking perspective.

Additional feedback locking work by Middlemas et al. (2020) showed that the cloud feedback outside of the Arctic contributes most to Arctic warming. This finding suggests an important non-local mechanism through which clouds contribute to Arctic amplification, which is not accounted for in the traditional feedback-forcing framework. Arguably, feedback locking shows the true impact of a climate feedback on the climate response as no process operates in isolation. Climate feedbacks instead influence one another and interact with other parts of the climate system, such as atmospheric heat transport, to determine the overall climate response. A limitation of feedback locking, when applied to the full range of climate feedbacks, is that the warming contributions from individual feedbacks do not fully account for the total warming, as interactions between feedbacks also play a role. Still, it is unclear if other climate models exhibit similar behavior as the CESM1-CAM5 simulations with inactive clouds. Moreover, it is unclear which region controls the cloud-induced Arctic amplification. Given that the cloud feedback is the primary source of uncertainty in future climate projections (Soden and Held, 2006; Dufresne and Bony, 2008; Schneider et al., 2017; Zelinka et al., 2017, 2020) and exhibits considerable intermodel spread at regional scales (Ceppi et al., 2017; Zelinka et al., 2020), it is imperative to reconcile these two perspectives and holistically quantify the contribution of clouds to Arctic amplification.

In this study, we quantify the influence of clouds on Arctic amplification by introducing a framework that unites the traditional feedback-forcing method with the feedback locking method. We first show that the cloud feedback contributes to Arctic amplification in CESM1-CAM5 by interacting with other climate feedbacks. Specifically, the surface temperature change resulting from including the cloud feedback is amplified by the surface-albedo, Planck, and lapse-rate feedbacks. We then show that a one-dimensional moist energy balance model (MEBM) exhibits similar behavior as CESM1-CAM5 and indicates that Arctic amplification from cloud-locking experiments results from including the mid-latitude cloud feedback. We use the MEBM as a surrogate model to quantify cloud feedback locking across a broader suite of climate models from CMIP5 and CMIP6 and show that the mid-latitude cloud feedback also contributes significantly to the intermodel spread in Arctic amplification across climate models. These results confirm that clouds can contribute to Arctic amplification and suggest that reducing the intermodel spread in the mid-latitude cloud feedback will reduce the intermodel spread in Arctic amplification. More broadly, these results highlight the need to better understand the interactions between climate feedbacks and their impact on surface temperature change.

2. Data and Methods

2.1. CESM1-CAM5 experiments

We analyze a set of CESM1-CAM5 (Hurrell et al., 2013) simulations in which the cloud radiative feedback was disabled (Chalmers et al., 2022). Briefly, two pairs of simulations are used. In the first pair, atmospheric carbon-dioxide concentrations are abruptly doubled (abrupt-2xCO2) from pre-industrial control (piControl) levels and held constant for 150 years. The second pair of simulations are a repeat of the first pair but with the cloud radiative feedback disabled (Middlemas et al., 2020; Chalmers et al., 2022). The cloud radiative feedback is disabled by prescribing cloud radiative properties at 2-hourly timesteps from a neutral El Niño-Southern Oscillation piControl year in the atmospheric model radiation calculations, while leaving the rest of the climate system to freely evolve. The abrupt-2xCO2 cloud-locked simulation is compared with a piControl cloud-locked simulation. For more detailed information, see Chalmers et al. (2022).

We use the values of $\mathcal{F}$ and λ calculated in Chalmers et al. (2022). The individual components of λ are calculated using the radiative-kernel method (Soden and Held, 2006; Shell et al., 2008; Soden et al., 2008) with CESM1-CAM5 radiative kernels (Pendergrass et al., 2018). Following Pendergrass et al. (2018), each radiative feedback is found by taking the difference in the climate variable between the fully-coupled piControl and fully-coupled abrupt-2xCO2 simulations, and multiplying the variable by the respective radiative kernel. $\mathcal{F}$ is calculated from abrupt-2xCO2 simulations under fixed-SST conditions (Smith et al., 2020). The other variables, ΔT, ΔG, and $\Delta(\nabla \cdot F)$, are calculated as the change between years 100 – 150 in the abrupt-2xCO2 simulations and the piControl simulations. ΔT is calculated as the change in near-surface air temperature, ΔG is calculated as the change in net surface heat fluxes, and $\Delta(\nabla \cdot F)$ is calculated as the change in the difference between the net top-of-atmosphere and net surface heat fluxes. All variables are annual averages.

2.2. CMIP5 and CMIP6 output

To examine the impact of cloud feedback locking in a broader suite of climate models, we use all CMIP5 (Taylor et al., 2012) and CMIP6 (Eyring et al., 2016) climate models that provide monthly output from the piControl and abrupt-4xCO2 simulations and the necessary variables to calculate annual averages of $\mathcal{F}$, λ, ΔT, ΔG, and $\Delta(\nabla \cdot F)$.

We use the values of $\mathcal{F}$ and λ calculated in Hahn et al. (2021). Briefly, the individual components of λ are calculated using the radiative-kernel method (Soden and Held, 2006; Shell et al., 2008; Soden et al., 2008) with CESM1-CAM5 radiative kernels (Pendergrass et al., 2018). We also use the individual components of λ calculated with other radiative kernels as detailed in Hahn et al. (2021) to assess the sensitivity to radiative kernel choice. These include radiative kernels from Soden et al. (2008), Shell et al. (2008), Block and Mauritsen (2013), Huang et al. (2017), and Smith et al. (2018). For more detailed information, see Hahn et al. (2021).

Each feedback is found by taking the difference in the climate variable of the abrupt-4xCO2 simulations and the concurrent piControl climatology and multiplying the variable by the respective radiative kernel. Note that the difference is a 31-year climatology centered on year-100 of each simulation. A 21-year running average is also applied to the piControl simulations to account for model drift before computing anomalies between abrupt-4xCO2 and piControl simulations. This helps to isolate anomalies due to greenhouse-gas forcing rather than model drift. $\mathcal{F}$ is calculated as the y-intercept of the regression between top-of-atmosphere radiation anomalies at each grid point against the global-mean ΔT for the first 20 years after abrupt-4xCO2 (Gregory et al., 2004). This calculation of $\mathcal{F}$ is different from the calculation of $\mathcal{F}$ from the CESM1-CAM5 simulations because not all climate models provide fixed-SST carbon-dioxide quadrupling experiments. Smith et al. (2020) noted that this 20-year regression produces $\mathcal{F}$ values that closely match methods using fixed sea-surface temperatures (Hansen et al., 2005). Note that this method for calculating λ includes both the true temperature-mediated feedbacks and the rapid adjustments that occur immediately upon carbon-dioxide quadrupling. However, it is important to note that locking the cloud feedback that contains rapid cloud adjustments in a MEBM, as done in this study, is akin to disabling the entire cloud feedback in a climate model.

The other variables, ΔT, ΔG, and $\Delta(\nabla \cdot F)$, are calculated as the 31-year climatological change centered on year-100 in the fully-coupled abrupt-4xCO2 simulations relative to the fully-coupled piControl simulations (after removing the model drift). ΔT is calculated as the change in near-surface air temperature, ΔG is calculated as the change in net surface heat fluxes, and $\Delta(\nabla \cdot F)$ is calculated as the change in the difference between the net top-of-atmosphere and net surface heat fluxes.

2.3. Moist energy balance model (MEBM)

To perform cloud feedback locking across a broader suite of climate models, we simulate zonal-mean ΔT using a MEBM with prescribed CMIP5 and CMIP6 output. MEBMs have been shown to effectively emulate zonal-mean ΔT from climate models under greenhouse gas forcing (Flannery, 1984; Hwang and Frierson, 2010; Roe et al., 2015; Siler et al., 2018; Bonan et al., 2018; Armour et al., 2019; Bonan et al., 2023). MEBMs assume the change in poleward atmospheric energy transport ΔF is proportional to the change in the meridional gradient of near-surface moist static energy $\Delta h = c_p \Delta T + L_v \Delta q$, where $c_p = 1005$ J kg^{-1} K^{-1} is the specific heat of air, $L_v = 2.5 \times 10^6$ J kg^{-1} is the latent heat of vaporization, and Δq is the change in near-surface specific humidity (assuming fixed relative humidity of 80%). This gives

$$\Delta F = -\frac{2\pi p_s}{g} D \left(1 - x^2\right) \frac{d\Delta h}{dx}, \tag{3}$$

where $p_s = 1000$ hPa is the surface air pressure, $g = 9.81$ m s^{-2} is the gravitational acceleration, D is a constant diffusion coefficient (with units of m^2 s^{-1}), x is the sine of the latitude, and $1 - x^2$ accounts for the spherical geometry of Earth.

On long timescales, the change in net heating of the atmosphere must balance the divergence of ΔF, resulting in

$$\mathcal{F} + \sum_i \lambda_i \Delta T - \Delta G = \Delta(\nabla \cdot F), \tag{4}$$

which is a single differential equation that can be solved numerically for ΔT and ΔF given zonal-mean profiles of $\mathcal{F}$, λ, and ΔG and a value (or zonal-mean profile) of D. Note that we have written λ as the sum of all individual radiative feedbacks, including λ_0. We set $D = 1.02 \times 10^6$ m^2 s^{-1}, which is the multi-model mean value from the pre-industrial control simulations. Changes in the magnitude and pattern of D have been shown to not significantly affect zonal-mean ΔT (Chang and Merlis, 2023; Ge et al., 2024).

Following Beer and Eisenman (2022) and Bonan et al. (2024), cloud feedback locking in the MEBM is performed by taking the cloud feedback that is diagnosed from climate model output, removing it from Eq. (4) and then solving for ΔT and ΔF. We perform cloud feedback locking across the global domain and regional domains. Note that in this MEBM, $\mathcal{F}$ and ΔG cannot change when the cloud feedback is locked since $\mathcal{F}$ and ΔG are prescribed based on climate model output. However, as discussed below, the change in $\mathcal{F}$ and ΔG when the cloud feedback is locked in a comprehensive climate model has little impact on the surface temperature change in the Arctic and Tropics. The zonal-mean ΔT attributed to including the cloud feedback in the MEBM can be found by taking the difference between the normal MEBM, where all feedbacks are active and the locked MEBM, where the cloud feedback is locked.

3. Climate feedback interactions and Arctic amplification

We begin by introducing a framework that reconciles the traditional feedback-forcing and feedback locking approaches. The two approaches can be reconciled by applying

Eq. (1) to the normal greenhouse-gas forcing simulation and the one in which the cloud feeback was disabled. We denote the normal greenhouse-gas forcing simulation as n and the cloud-locked greenhouse-gas forcing simulation as l. Thus, the difference of any variable χ between the two simulations can be expressed as

$$\chi_{n-l} = \chi_n - \chi_l. \tag{5}$$

By applying Eq. (1) to the two simulations and taking the difference, while also noting that Eq. (5) can be rearranged such that $\chi_l = \chi_n - \chi_{n-l}$, we can derive a diagnostic equation that expresses cloud-induced surface temperature change ΔT_{n-l} as

$$\Delta T_{n-l} = \frac{1}{\lambda_0}\left(-\underbrace{\mathcal{F}_{n-l}}_{\text{(a)}} - \underbrace{\lambda_{n-l}\Delta T_n}_{\text{(b)}} - \underbrace{\lambda_l \Delta T_{n-l}}_{\text{(c)}} + \underbrace{\Delta G_{n-l}}_{\text{(d)}} + \underbrace{\Delta(\nabla \cdot F)_{n-l}}_{\text{(e)}} - \underbrace{\epsilon_{n-l}}_{\text{(f)}} \right), \tag{6}$$

where each term is a partial temperature contribution to ΔT_{n-l}, with (a) denoting interactions between clouds and radiative forcing, (b) denoting the change in the net radiative feedback, (c) denoting interactions between cloud-induced temperature change and other radiative feedbacks, (d) denoting interactions between clouds and ocean heat uptake, (e) denoting interactions between clouds and atmospheric heat transport, and (f) denoting the residual term. Note that if only the cloud feedback were disabled and no other component of the climate system were to change, the cloud feedback contribution diagnosed from the traditional feedback-forcing framework would be equal to Eq. (6) through Term (b). However, in what follows, we will show that Term (c), which denotes interactions between other radiative feedbacks, significantly contributes to Eq. (6). Note that λ_l is defined in Eq. (2) and does not contain λ_0.

In the Arctic, ΔT_{n-l} is larger when compared to the Tropics primarily because of Term (c), which denotes ΔT_{n-l} resulting from interactions between the cloud-induced surface temperature change and other radiative feedbacks (cyan dot, left panel, Fig. 2a). A breakdown of λ_l into individual radiative feedback components shows that this amplification occurs primarily because of the surface-albedo, Planck, and lapse-rate feedbacks (cyan symbols, Fig. 2b). In other words, the cloud-induced temperature change is amplified by the surface-albedo, Planck, and lapse-rate feedbacks in the Arctic. Term (b), which denotes ΔT_{n-l} due to changes in the net radiative feedback, approximates the diagnostic contribution of the cloud feedback quite well (compare right purple triangle in Fig. 1a and red dot in Fig. 2a). In fact, Term (b) suggests a warming contribution of approximately 0.5 K in the Tropics and 0 K in the Arctic (Fig. 2a) and the diagnostic approach suggests a warming contribution of approximately 0.4 K in the Tropics and 0 K in the Arctic (Fig. 1a). This occurs because the other individual radiative feedbacks change very little (red symbols, Fig. 2b). Most of the change in the net radiative feedback occurs because of the disabled cloud feedback (sideways red triangle, Fig. 2b) and the lapse-rate and water-vapor feedbacks cancel each other out (upward and downward red triangles, Fig. 2b). Note that for these regional domains, $\mathcal{F}$ and ΔG change very little with a disabled cloud feedback, meaning Terms (a) and (d) in Eq. (6) are approximately zero. Similar results are obtained when comparing Arctic surface temperature change to a global average (not shown).

The above result shows that the difference between the traditional feedback-forcing framework, which suggests that clouds contribute little to warming in the Arctic and Tropics, and the feedback-locking approach, which suggests that clouds contribute significantly to warming in the Arctic and Tropics, can be attributed to climate feedback interactions. In the Arctic, the cloud-induced surface temperature change is amplified by the surface-albedo, Planck, and lapse-rate feedbacks, which change very little in response to an inactive cloud feedback. In the Tropics, the cloud feedback as diagnosed from the traditional-feedback forcing accounts for most of cloud-induced warming as suggested by cloud feedback locking.

3.1. Cloud feedback locking in an energy balance model

3.1.1. Comparison to CESM1-CAM5 Can the results of cloud feedback locking from a single climate model be trusted? The CESM1-CAM5 simulations suggest that an active cloud feedback contributes to Arctic amplification. However, the cloud feedback shows considerable intermodel spread at both global (Soden and Held, 2006; Dufresne and Bony, 2008; Schneider et al., 2017; Zelinka et al., 2017, 2020) and regional (Ceppi et al., 2017; Zelinka et al., 2020) scales. This spread implies that cloud feedback locking in other climate models could yield different climate responses. Nonetheless, conducting cloud feedback locking across climate models is challenging due to its computational cost and the substantial differences in cloud model components.

In recent years, a number of studies have shown that one-dimensional MEBMs, which simulate atmospheric heat transport as downgradient diffusion of near-surface moist-static energy, capture the behavior of climate models under greenhouse-gas forcing, including the magnitude of Arctic amplification (Roe et al., 2015; Bonan et al., 2018; Siler et al., 2018; Feldl and Merlis, 2021). This suggests that MEBMs can serve as surrogate models for exploring the impact of cloud feedback locking on Arctic amplification. However, it remains unclear whether the simplicity of MEBMs affects their ability to accurately replicate the behavior of CESM1-CAM5 with locked cloud feedback. Note that Beer and Eisenman (2022) conducted feedback locking experiments in a MEBM but did not examine whether it produces similar behavior as a comprehensive climate model. Here, we compare cloud feedback locking in a MEBM to the CESM1-CAM5 abrupt-2xCO2 simulation with an inactive cloud feedback. Because the other radiative feedbacks in CESM1-CAM5 change very little in response to an inactive cloud feedback (red symbols, Fig. 2b), we hypothesize that removing the cloud feedback from a MEBM will result in a similar response as the cloud-locked CESM1-CAM5 simulations.

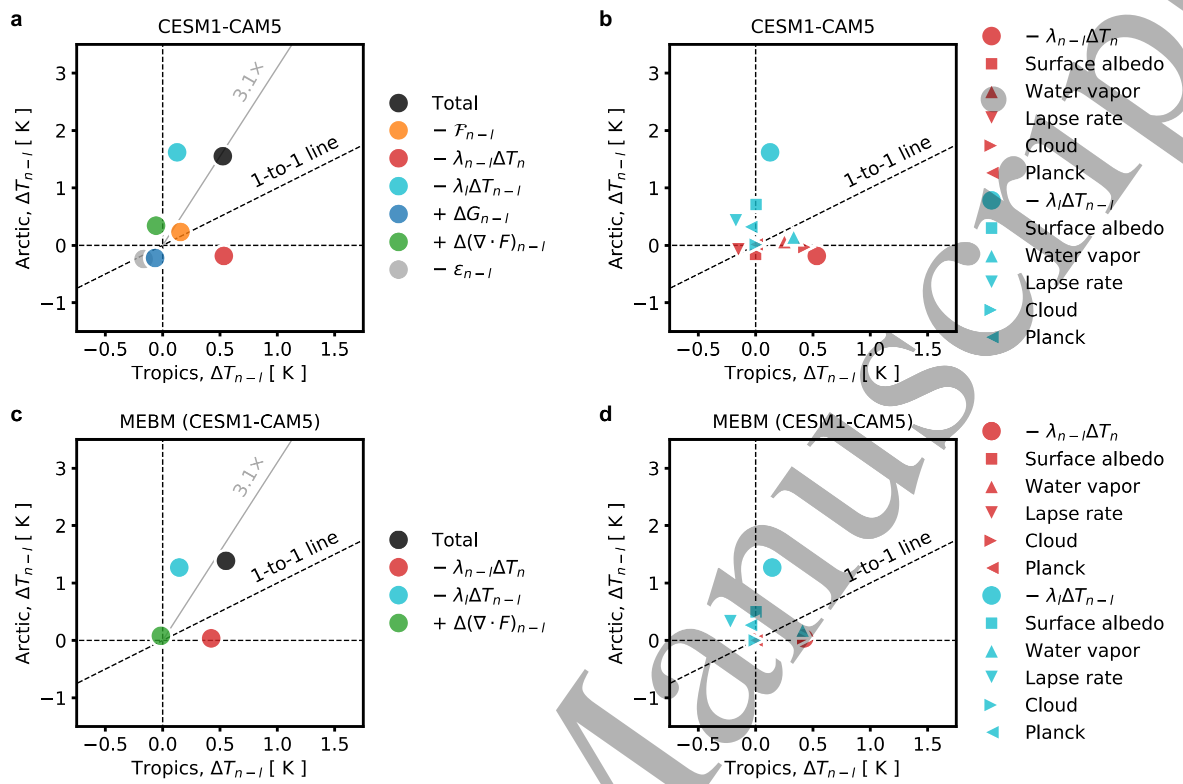

Figure 2. Contributions to cloud-induced Arctic amplification. Contributions to cloud-induced surface temperature change ΔT_{n-l} in the (x-axis) Tropics (30°S-30°N) and (y-axis) Arctic (60°N-90°N) for CESM1-CAM5 abrupt-2xCO2 simulations. Panel (a) denotes each mechanism in Eq. (6). The colored dots sum to the black dot. The orange dot denotes interactions with radiative forcing, the red dot denotes changes in radiative feedbacks, the cyan dot denotes interactions between other radiative feedbacks, the blue dot denotes interactions with ocean heat uptake, and the green dot denotes interactions with atmospheric heat transport. Panel (b) shows the individual radiative feedbacks for the red and cyan dots in the left panel. The red and cyan squares and triangles sum to the red and cyan dots, respectively. Panel (c) and panel (d) are the same as panel (a) and panel (b) but based on including the CESM1-CAM5 abrupt-2xCO2 cloud feedback in the MEBM. The grey lines and numbers in the left panels of (a) and (c) indicate the magnitude of Arctic amplification from the normal abrupt-2xCO2 CESM1-CAM5 simulation.

MEBM cloud feedback locking is performed by removing the prescribed cloud feedback based on CESM1-CAM5 output and comparing it to a standard MEBM simulation in which all CESM1-CAM5 output is prescribed, thus activating all feedbacks. Eq. (3) is applied to the MEBM simulations, but note that $\mathcal{F}$ and ΔG cannot change when the cloud feedback is locked, since they are prescribed. As a result, Terms (a) and (d) in Eq. (3) are zero when using the MEBM.

The MEBM accurately simulates the cloud-induced Arctic amplification suggested by the CESM1-CAM5 cloud-locked simulations (Fig. 2c). The MEBM produces a cloud-induced Arctic-to-Tropics warming ratio that is slightly smaller than the CESM1-CAM5 cloud-induced Arctic-to-Tropics warming ratio of 3.1. However, the MEBM shows that cloud-induced Arctic amplification occurs because of Term (c), which describes the interaction between cloud-induced surface temperature changes and the surface-albedo, Planck, and lapse-rate feedbacks (cyan dots, Fig. 2c-d). This finding is consistent with the CESM1-CAM5 simulations.

The success of the MEBM in emulating the CESM1-CAM5 cloud locking experiments suggests the MEBM can be used to examine how the cloud feedback in different regions affects Arctic amplification. Middlemas et al. (2020) showed that the cloud feedback outside of the Arctic contributes most to the cloud-induced Arctic warming. But it is still unclear which region outside of the Arctic is contributing most to the cloud-induced Arctic warming. To examine this, we use the MEBM to lock the cloud feedback in four different regional domains, spanning 30° latitude bands from 90°N to 30°S.

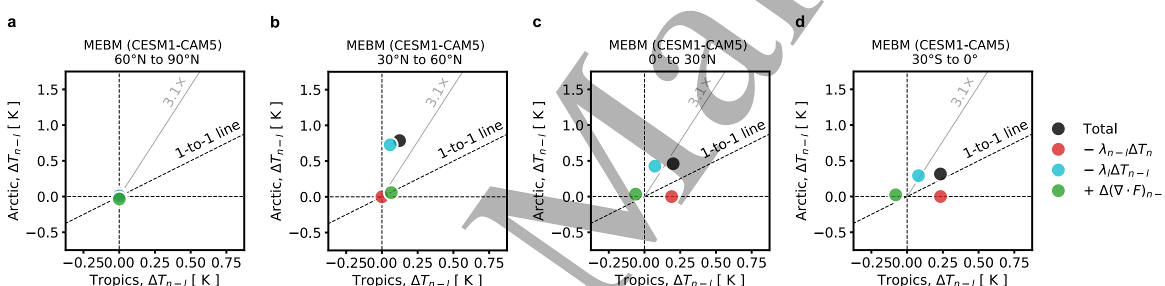

Figure 3. Impact of regional cloud locking on Arctic amplification. Contributions to cloud-induced surface temperature change ΔT_{n-l} in the (x-axis) Tropics (30°S-30°N) and (y-axis) Arctic (60°N-90°N) based on including the cloud feedback in the MEBM that is diagnosed from the CESM1-CAM5 abrupt-2xCO2 simulation. Each panel denotes when the cloud feedback was included from (a) 60°N to 90°N, (b) 30°N to 60°N, (c) 0° to 30°N, and (d) 30°S to 0°. Each dot denotes a mechanism in Eq. (6). The colored dots sum to the black dot. The red dot denotes changes in radiative feedbacks, the cyan dot denotes interactions between other radiative feedbacks, and the green dot denotes interactions with atmospheric heat transport. The grey line and number in each panel indicate the magnitude of Arctic amplification from the normal abrupt-2xCO2 CESM1-CAM5 simulation.

The MEBM suggests the mid-latitude (30°N-60°N) cloud feedback contributes most to the cloud-induced Arctic amplification (black dot, Fig. 3b). When the mid-latitude cloud feedback is included, the Arctic warms by 0.8 K while the Tropics warm by 0.1 K, producing an Arctic-to-Tropics warming ratio of 8. This warming is also related almost entirely to Term (c), the interaction of the cloud-induced warming with other climate feedbacks local to the Arctic (cyan dot, Fig. 3b). The Arctic (60°N-90°N) cloud feedback contributes little to Arctic amplification (black dot, Fig. 3a)—consistent with Middlemas et al. (2020). Cloud feedbacks in the Tropics (30°S-30°N) contribute some to Arctic warming but little to Arctic amplification (black dots, Fig. 3c-d). Across all regions, the interaction of the cloud-induced warming with other radiative feedbacks is the primary contributor to Arctic warming and Arctic amplification (cyan dots, Fig. 3).

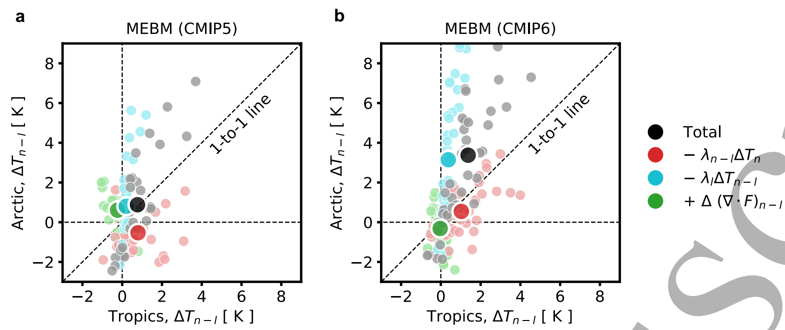

Figure 4. Global cloud locking in CMIP5 and CMIP6. Contributions to cloud-induced surface temperature change ΔT_{n-l} in the (x-axis) Tropics (30°S-30°N) and (y-axis) Arctic (60°N-90°N) based on including the cloud feedback globally in the MEBM that is diagnosed from (a) CMIP5 and (b) CMIP6. Each dot denotes a mechanism in Eq. (6). The colored dots sum to the black dot. The red dots denote changes in radiative feedbacks, the cyan dots denote interactions between other radiative feedbacks, and the green dots denote interactions with atmospheric heat transport. The large dots denote the multi-model mean and the small dots denote an individual CMIP5 and CMIP6 climate model.

3.1.2. Cloud locking in CMIP5 and CMIP6 Having shown that the MEBM emulates the CESM1-CAM5 cloud locking experiments and that the mid-latitude cloud feedback contributes most to Arctic amplification, we now examine the impact of cloud feedback locking on Arctic amplification across broader range of climate models. To do this, we conduct the same analyses as above with the CESM1-CAM5 simulations but with a broader suite of CMIP5 and CMIP6 climate models under abrupt-4xCO2 (see Section 2.2). More specifically, we perform a normal MEBM simulation by prescribing the patterns of $\mathcal{F}$, λ and ΔG from each CMIP5 and CMIP6 climate model in the MEBM and compare that to a MEBM simulation in which the cloud feedback diagnosed from each climate model is removed. We then calculate the terms in Eq. (3) for the MEBM simulations.

When the cloud feedback is included in the MEBM globally, there is large surface temperature change in the Arctic and Tropics (Fig. 4). On average, CMIP5 climate models exhibit a cloud-induced warming of approximately 1 K in both the Tropics and Arctic (Fig. 4a), while CMIP6 climate models exhibit more warming in the Arctic of approximately 3.5 K (Fig. 4b). CMIP6 climate models exhibit stronger cloud-induced Arctic warming than CMIP5 climate models because of less negative Arctic cloud feedbacks (red dots, Fig. 4), which has been noted previously by Hahn et al. (2021), and because of stronger climate feedback interactions (cyan dots, Fig. 4). The less-negative cloud feedbacks are related to a less-negative shortwave low-cloud amount and scattering feedbacks (Zelinka et al., 2020). However, there is considerable intermodel spread in the amount of cloud-induced Arctic surface temperature change across CMIP5 and CMIP6 (Fig. 4). For example, in CMIP5, the cloud-induced surface temperature change results in a temperature range of -2 K to 8 K in the Arctic (grey dots, Fig. 4a). In CMIP6, the cloud-induced surface temperature change results in an even larger temperature range of -2 K to 10 K in the Arctic (grey dots, Fig. 4b). Similar to the CESM1-CAM5 simulations, the intermodel spread in surface temperature change in the Arctic under cloud locking is primarily associated with Term (c), which represents climate feedback interactions (cyan dots, Fig. 4). In contrast, the intermodel spread in surface temperature change in the Tropics under cloud locking is mainly linked to the cloud feedback itself (red dots, Fig. 4).

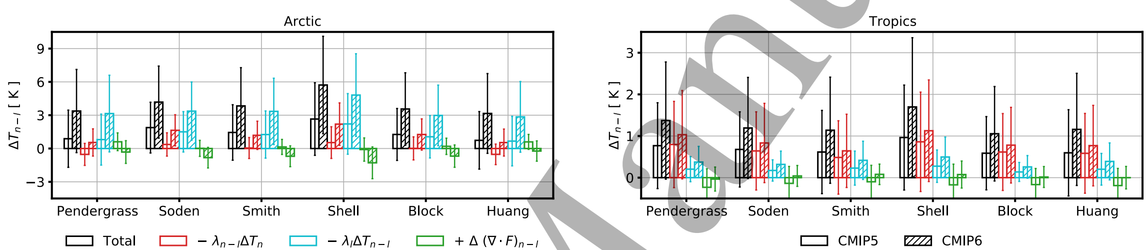

Figure 5. Sensitivity of global cloud locking to radiative kernels. Contributions to cloud-induced surface temperature change ΔT_{n-l} in the (left) Arctic (60°N-90°N) and (right) Tropics (30°S-30°N) based on including the cloud feedback globally in the MEBM and using feedbacks derived from various radiative kernels. Each bar denotes a mechanism in Eq. (6). The colored bars sum to the black bars. The red bars denote changes in radiative feedbacks, the cyan bars denote interactions between other radiative feedbacks, and the green bars denote interactions with atmospheric heat transport. The errorbars denote a ± one standard deviation of all MEBM simulations. The open bars denote CMIP5 and the hatched bars denote CMIP6. Note that the y-axis limits differ between the left and right panels.

Global cloud locking in the MEBM, based on CMIP5 and CMIP6 feedbacks derived from different radiative kernels, produces similar results (Fig. 5). However, some radiative kernels indicate greater warming from cloud locking, particularly in the Arctic (black bars, Fig. 5). For instance, when CMIP5 and CMIP6 feedbacks are estimated using radiative kernels from Shell et al. (2008), cloud locking results in more Arctic warming when compared to the Pendergrass et al. (2018) radiative kernels (left panel, black bars, Fig. 5). This occurs because of differences in Term (b), which describes the Arctic cloud feedback itself, and Term (c), which describes feedbacks interactions (left panel, red and cyan bars, Fig. 5). In the Tropics, global cloud locking in the MEBM shows similar behavior across feedbacks derived from different radiative kernels (right panel, Fig. 5).

When the cloud feedback is included in different regional domains, the impact on surface temperature change becomes even more striking. In contrast to the MEBM cloud feed-

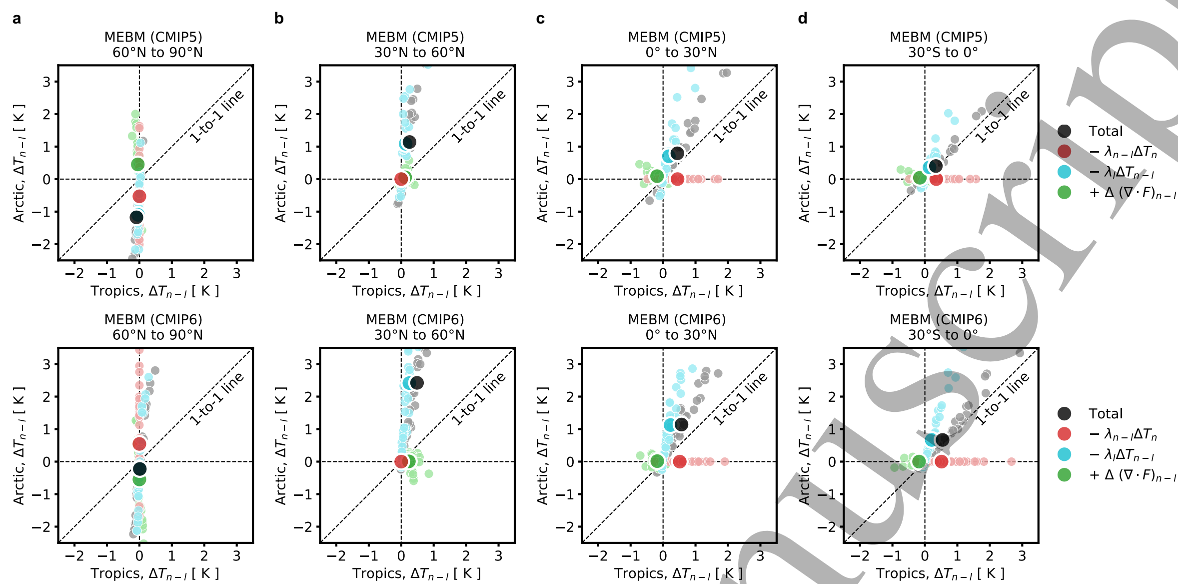

Figure 6. Impact of regional cloud locking on Arctic amplification in CMIP5 and CMIP6. Contributions to cloud-induced surface temperature change ΔT_{n-l} in the (x-axis) Tropics (30°S-30°N) and (y-axis) Arctic (60°N-90°N) based on including the cloud feedback from (a) 60°N to 90°N, (b) 30°N to 60°N, (c) 0° to 30°N, and (d) 30°S to 0° in the MEBM. The feedbacks are derived from (top) CMIP5 and (bottom) CMIP6 output. Each dot denotes a mechanism in Eq. (6). The colored dots sum to the black dot. The red dots denote changes in radiative feedbacks, the cyan dots denote interactions between other radiative feedbacks, and the green dots denote interactions with atmospheric heat transport. The large dots denote the multi-model mean and the small dots denote an individual CMIP5 and CMIP6 climate model.

back locking with CESM1-CAM5 output, MEBM cloud feedback locking with CMIP5 and CMIP6 output indicates a more diverse range of surface temperature changes in the Arctic and Tropics (Fig. 6). Both CMIP5 and CMIP6 climate models suggest on average the Arctic warms little or cools slightly when the Arctic (60°N-90°N) cloud feedback is included, but there is a large intermodel spread that ranges from -2 K to 3 K (Fig. 6a). Still, the mid-latitude (30°N-60°N) cloud feedback contributes most to the cloud-induced Arctic amplification (Fig. 6b). CMIP5 and CMIP6 climate models suggest that on average, the mid-latitude cloud feedback contributes to an Arctic-to-Tropics warming ratio of 5–6, with substantial intermodel spread that is solely related to Term (c), which describes feedback interactions (cyan dots, Fig. 6b). As with CESM1-CAM5, including the cloud feedback from 30°S-30°N does not contribute much to Arctic amplification but does contribute strongly to warming in both the Arctic and Tropics (Fig. 6c-d), consistent with Bonan et al. (2018). The cloud-induced surface temperature in the Tropics occurs primarily because of Term (b), which describes the cloud feedback itself (red dots, Fig. 6c-d).

Regional cloud locking performed in the MEBM using CMIP5 and CMIP6 feedbacks derived from different radiative kernels produces similar results, indicating that mid-latitude cloud feedback significantly contributes to Arctic warming and Arctic amplifi-

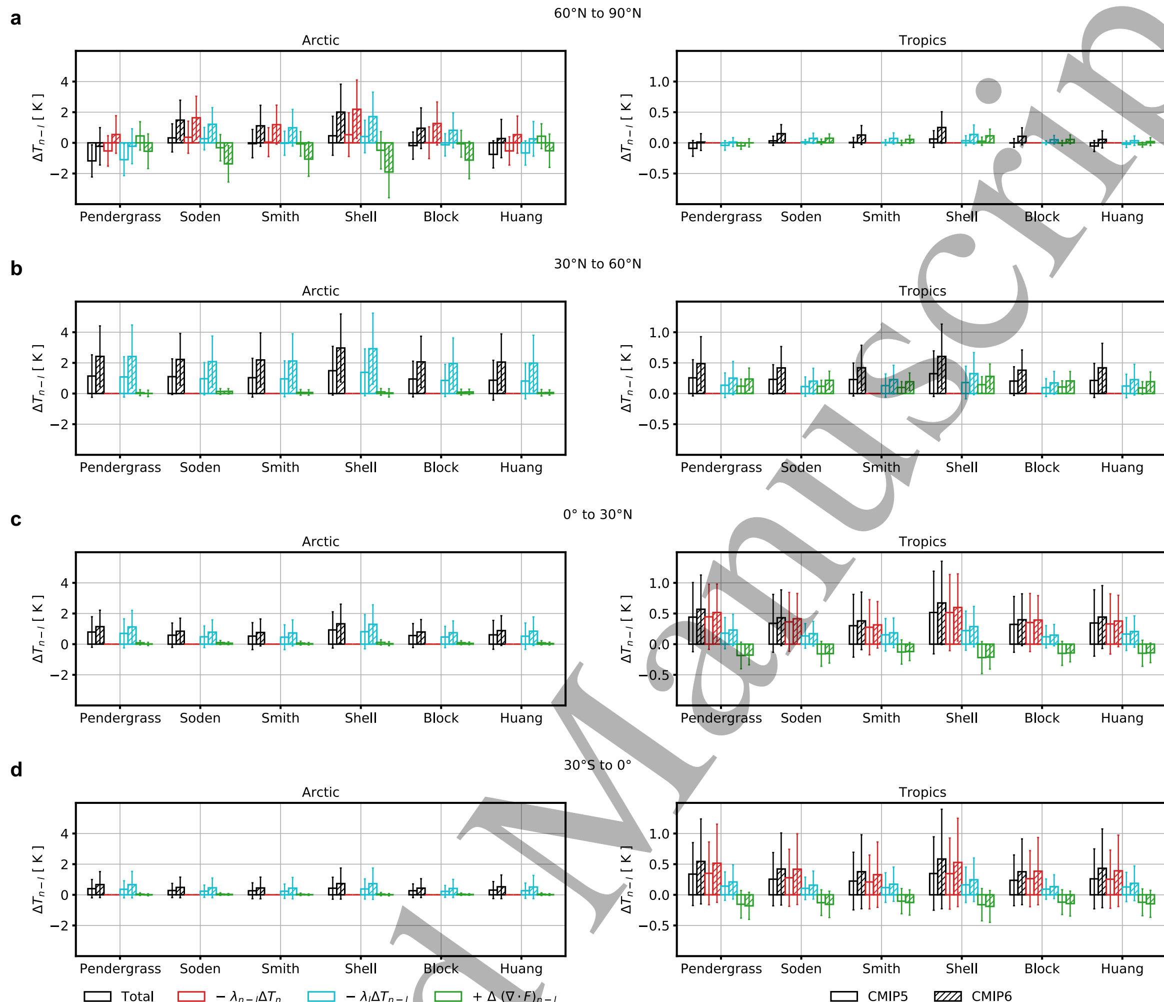

Figure 7. Sensitivity of regional cloud feedback locking to radiative kernels. Contributions to cloud-induced surface temperature change ΔT_{n-l} in the (left) Arctic (60°N-90°N) and (right) Tropics (30°S-30°N) based on including the cloud feedback from (a) 60°N to 90°N, (b) 30°N to 60°N, (c) 0° to 30°N, and (d) 30°S to 0° in the MEBM and using feedbacks derived from various radiative kernels. Each bar denotes a mechanism in Eq. (6). The colored bars sum to the black bars. The red bars denote changes in radiative feedbacks, the cyan bars denote interactions between other radiative feedbacks, and the green bars denote interactions with atmospheric heat transport. The errorbars denote a ± one standard deviation of all MEBM simulations. The open bars denote CMIP5 and the hatched bars denote CMIP6. Note that the y-axis limits differ between the left and right panels.

425 cation (Fig. 7b). However, as with global cloud locking, the results can vary depending
426 on the specific radiative kernels used to estimate individual feedbacks. For instance,
427 CMIP5 and CMIP6 feedbacks derived from some radiative kernels (e.g., Soden et al.,
428 2008; Shell et al., 2008) result in strong Arctic warming when the Arctic cloud feedback
429 is included (left panel, Fig. 7a). In contrast, this effect is not observed with feedbacks
430 based on radiative kernels from Pendergrass et al. (2018) or Huang et al. (2017). This
431 discrepancy arises primarily because of Term (b), which shows that the Arctic cloud
432 feedback is more positive with the Soden et al. (2008) and Shell et al. (2008) radia-

tive kernels, and because of Term (c), which shows that feedback interactions are also stronger (red and cyan bars, Fig. 7a). In the Tropics, regional cloud locking results in similar amounts of warming across feedbacks derived from different radiative kernels (Fig. 7c-d).

4. Discussion and conclusions

This study has several key findings. First, we reconciled two different perspectives on how climate feedbacks influence surface temperature change. In particular, we show the traditional feedback-forcing framework (e.g., Pithan and Mauritsen, 2014; Hahn et al., 2021), which suggests that the cloud feedback contributes little to warming in the Arctic, can be reconciled with the feedback locking framework (e.g., Middlemas et al., 2020; Chalmers et al., 2022), which suggests that clouds contribute significantly to warming in the Arctic, by accounting for interactions with other climate feedbacks. In the Tropics, the cloud feedback contribution diagnosed using the traditional feedback-forcing framework is similar to the contribution from feedback locking, indicating that the traditional feedback-forcing framework works well in estimating the cloud warming contribution for tropical regions. Second, we showed that a MEBM with no cloud feedback exhibits similar behavior as a coupled climate model with a disabled cloud feedback (Fig. 2), which suggests that MEBMs can be used to examine the impact of feedback locking on other climate processes. Finally, we showed that the mid-latitude cloud feedback contributes to Arctic amplification by interacting with other climate feedbacks. The surface temperature change resulting from including the mid-latitude cloud feedback is amplified in the Arctic by the surface-albedo, Planck, and lapse-rate feedbacks (Fig. 3).

Our study underscores the uncertain role of the Arctic cloud feedback in Arctic climate change. Middlemas et al. (2020) used CESM1-CAM5 to show that including the Arctic cloud feedback under greenhouse gas forcing has minimal impact on Arctic warming. In contrast, our analysis across a broader suite of climate models shows that including the Arctic cloud feedback can result in either large cooling or large warming (Fig. 6). We also found that the magnitude of Arctic surface temperature change with MEBM-based cloud locking depends on the specific radiative kernels used to diagnose individual feedbacks (Fig. 7), adding complexity to understanding the role of Arctic cloud feedback in climate change. Some of the differences in surface albedo and shortwave cloud feedbacks across radiative kernels could potentially be reconciled by applying the approximate partial radiative perturbation (APRP) technique (Taylor et al., 2007; Morrison et al., 2019; Chalmers et al., 2022). Of course, our results may already be biased because contemporary climate models exhibit substantial cloud biases, leading to underestimation of both Arctic and non-Arctic cloud feedbacks (Tan and Storelvmo, 2019; Morrison et al., 2019; Cesana et al., 2021; Mülmenstädt et al., 2021; Tan et al., 2022, 2023). For example, Tan and Storelvmo (2019) showed that correcting biases in the representation of supercooled liquid in mixed-phase clouds globally can either enhance or reduce Arctic amplification, depending on the microphysical cloud characteristics. This highlights the need to improve our understanding and constraints on both Arctic and non-Arctic cloud feedbacks, as they likely play a critical role in determining the magnitude of Arctic amplification.

While the feedback-locking framework does not alleviate concerns about climate model biases, it does help offer an approach to assess how other components of the climate system interact to shape the patterns of climate change. For example, diagnostic assessments indicate that ocean heat transport contributes little to Arctic amplification (Pithan and Mauritsen, 2014; Feldl et al., 2020; Hahn et al., 2021). However, experiments in which ocean heat transport was disabled or unable to change suggest that ocean heat transport does contribute to Arctic amplification (Singh et al., 2017; Beer et al., 2020; England and Feldl, 2024). The feedback-locking framework implies that these two perspectives can likely be reconciled by accounting for climate system interactions. Applying this framework to other mechanism denial experiments might better indicate the factors influencing the climate response to external forcing and help to constrain future climate projections.

Importantly, our results demonstrate a non-local pathway for Arctic amplification and suggest that constraining the intermodel spread in the mid-latitude cloud feedback across contemporary climate models will reduce the intermodel spread in Arctic amplification. Arguably, the feedback locking approach demonstrates a more impactful way of reducing the intermodel spread in the climate response to greenhouse gas forcing, as no feedback process operates in isolation. Instead, climate feedbacks interact with each other and other components of the climate system, such as atmospheric heat transport, to shape the climate response. Further quantification of climate feedback interactions and assessment of their impact on other features of climate change should remain a focus of the climate science community.

Acknowledgements

The authors thank the climate modeling groups for producing and making available their model output, which is accessible at the Earth System Grid Federation (ESGF) Portal (`https://esgf-node.llnl.gov/search`). The CESM1-CAM5 model output is available on Globus Collection (/glade/campaign/univ/ucub0090/cloudlocking). D.B.B was supported by the National Science Foundation (NSF) Graduate Research Fellowship Program (NSF Grant DGE1745301). J.E.K. was supported by NSF Grant OPP-2233420. N.F. was supported by NSF Grant AGS-1753034. M.D.Z.'s work was supported by the U.S. Department of Energy (DOE) Regional and Global Model Analysis program area and was performed under the auspices of the U.S. DOE by Lawrence Livermore National Laboratory under contract DEAC52-07NA27344. Code for the moist energy balance model and sample CMIP output can be found at `https:`

//github.com/dave-bonan/energy-balance-models.

References

1. Armour, K. C., Siler, N., Donohoe, A., and Roe, G. H. (2019). Meridional atmospheric heat transport constrained by energetics and mediated by large-scale diffusion. *Journal of Climate*, 32(12):3655–3680.
2. Beer, E. and Eisenman, I. (2022). Revisiting the role of the water vapor and lapse rate feedbacks in the Arctic amplification of climate change. *Journal of Climate*, 35(10):2975–2988.
3. Beer, E., Eisenman, I., and Wagner, T. J. (2020). Polar amplification due to enhanced heat flux across the halocline. *Geophysical Research Letters*, 47(4):e2019GL086706.
4. Block, K. and Mauritsen, T. (2013). Forcing and feedback in the MPI-ESM-LR coupled model under abruptly quadrupled CO2. *Journal of Advances in Modeling Earth Systems*, 5(4):676–691.
5. Bonan, D. B., Armour, K. C., Roe, G. H., Siler, N., and Feldl, N. (2018). Sources of uncertainty in the meridional pattern of climate change. *Geophysical Research Letters*, 45(17):9131–9140.
6. Bonan, D. B., Feldl, N., Siler, N., Kay, J. E., Armour, K. C., Eisenman, I., and Roe, G. H. (2024). The influence of climate feedbacks on regional hydrological changes under global warming. *Geophysical Research Letters*, 51(3):e2023GL106648.
7. Bonan, D. B., Siler, N., Roe, G. H., and Armour, K. C. (2023). Energetic constraints on the pattern of changes to the hydrological cycle under global warming. *Journal of Climate*, 36(10):3499–3522.
8. Caldwell, P. M., Zelinka, M. D., Taylor, K. E., and Marvel, K. (2016). Quantifying the sources of intermodel spread in equilibrium climate sensitivity. *Journal of Climate*, 29(2):513–524.
9. Ceppi, P., Brient, F., Zelinka, M. D., and Hartmann, D. L. (2017). Cloud feedback mechanisms and their representation in global climate models. *Wiley Interdisciplinary Reviews: Climate Change*, 8(4):e465.
10. Cesana, G. V., Ackerman, A. S., Fridlind, A. M., Silber, I., and Kelley, M. (2021). Snow reconciles observed and simulated phase partitioning and increases cloud feedback. *Geophysical Research Letters*, 48(20):e2021GL094876.
11. Chalmers, J., Kay, J. E., Middlemas, E. A., Maroon, E. A., and DiNezio, P. (2022). Does disabling cloud radiative feedbacks change spatial patterns of surface greenhouse warming and cooling? *Journal of Climate*, 35(6):1787–1807.
12. Chang, C.-Y. and Merlis, T. M. (2023). The Role of Diffusivity Changes on the Pattern of Warming in Energy Balance Models. *Journal of Climate*, 36(22):7993–8006.
13. Chung, P.-C. and Feldl, N. (2024). Sea ice loss, water vapor increases, and their interactions with atmospheric energy transport in driving seasonal polar amplification. *Journal of Climate*, 37(8):2713–2725.
14. Crook, J. A., Forster, P. M., and Stuber, N. (2011). Spatial patterns of modeled climate feedback and contributions to temperature response and polar amplification. *Journal of Climate*, 24(14):3575–3592.
15. Dufresne, J.-L. and Bony, S. (2008). An assessment of the primary sources of spread of global warming estimates from coupled atmosphere–ocean models. *Journal of Climate*, 21(19):5135–5144.
16. England, M. R., Eisenman, I., Lutsko, N. J., and Wagner, T. J. (2021). The recent emergence of Arctic amplification. *Geophysical Research Letters*, 48(15):e2021GL094086.
17. England, M. R. and Feldl, N. (2024). Robust polar amplification in ice-free climates relies on ocean heat transport and cloud radiative effects. *Journal of Climate*, 37(7):2179–2197.

18. Eyring, V., Bony, S., Meehl, G. A., Senior, C. A., Stevens, B., Stouffer, R. J., and Taylor, K. E. (2016). Overview of the Coupled Model Intercomparison Project Phase 6 (CMIP6) experimental design and organization. *Geoscientific Model Development*, 9(5):1937–1958.
19. Feldl, N., Bordoni, S., and Merlis, T. M. (2017). Coupled high-latitude climate feedbacks and their impact on atmospheric heat transport. *Journal of Climate*, 30(1):189–201.
20. Feldl, N. and Merlis, T. M. (2021). Polar amplification in idealized climates: The role of ice, moisture, and seasons. *Geophysical Research Letters*, 48(17):e2021GL094130.
21. Feldl, N., Po-Chedley, S., Singh, H. K., Hay, S., and Kushner, P. J. (2020). Sea ice and atmospheric circulation shape the high-latitude lapse rate feedback. *NPJ Climate and Atmospheric Science*, 3(1):41.
22. Flannery, B. P. (1984). Energy balance models incorporating transport of thermal and latent energy. *Journal of Atmospheric Sciences*, 41(3):414–421.
23. Ge, Q., Zheng, Z., Kang, L., Donohoe, A., Armour, K., and Roe, G. (2024). The sensitivity of climate and climate change to the efficiency of atmospheric heat transport. *Climate Dynamics*, 62(3):2057–2067.
24. Goosse, H., Kay, J. E., Armour, K. C., Bodas-Salcedo, A., Chepfer, H., Docquier, D., Jonko, A., Kushner, P. J., Lecomte, O., Massonnet, F., et al. (2018). Quantifying climate feedbacks in polar regions. *Nature Communications*, 9(1):1919.
25. Graversen, R. G. and Wang, M. (2009). Polar amplification in a coupled climate model with locked albedo. *Climate Dynamics*, 33:629–643.
26. Gregory, J. M., Ingram, W. J., Palmer, M., Jones, G. S., Stott, P., Thorpe, R., Lowe, J. A., Johns, T., and Williams, K. (2004). A new method for diagnosing radiative forcing and climate sensitivity. *Geophysical Research Letters*, 31(3).
27. Hahn, L. C., Armour, K. C., Zelinka, M. D., Bitz, C. M., and Donohoe, A. (2021). Contributions to polar amplification in CMIP5 and CMIP6 models. *Frontiers in Earth Science*, 9:710036.
28. Hall, A. (2004). The role of surface albedo feedback in climate. *Journal of climate*, 17(7):1550–1568.
29. Hansen, J., Sato, M., Ruedy, R., Nazarenko, L., Lacis, A., Schmidt, G., Russell, G., Aleinov, I., Bauer, M., Bauer, S., et al. (2005). Efficacy of climate forcings. *Journal of Geophysical Research: Atmospheres*, 110(D18).
30. Henry, M., Merlis, T. M., Lutsko, N. J., and Rose, B. E. (2021). Decomposing the drivers of polar amplification with a single-column model. *Journal of Climate*, 34(6):2355–2365.
31. Holland, M. M. and Bitz, C. M. (2003). Polar amplification of climate change in coupled models. *Climate Dynamics*, 21(3):221–232.
32. Huang, Y., Xia, Y., and Tan, X. (2017). On the pattern of CO2 radiative forcing and poleward energy transport. *Journal of Geophysical Research: Atmospheres*, 122(20):10–578.
33. Hurrell, J. W., Holland, M. M., Gent, P. R., Ghan, S., Kay, J. E., Kushner, P. J., Lamarque, J.-F., Large, W. G., Lawrence, D., Lindsay, K., et al. (2013). The community earth system model: a framework for collaborative research. *Bulletin of the American Meteorological Society*, 94(9):1339–1360.
34. Hwang, Y.-T. and Frierson, D. M. (2010). Increasing atmospheric poleward energy transport with global warming. *Geophysical Research Letters*, 37(24).
35. Hwang, Y.-T., Frierson, D. M., and Kay, J. E. (2011). Coupling between Arctic feedbacks and changes in poleward energy transport. *Geophysical Research Letters*, 38(17).
36. Langen, P. L., Graversen, R. G., and Mauritsen, T. (2012). Separation of contributions from radiative feedbacks to polar amplification on an aquaplanet. *Journal of climate*, 25(8):3010–3024.
37. Manabe, S. and Stouffer, R. J. (1980). Sensitivity of a global climate model to an increase of CO2 concentration in the atmosphere. *Journal of Geophysical Research: Oceans*, 85(C10):5529–5554.

38. Manabe, S. and Wetherald, R. T. (1975). The effects of doubling the CO2 concentration on the climate of a general circulation model. *Journal of Atmospheric Sciences*, 32(1):3–15.
39. Mauritsen, T., Graversen, R. G., Klocke, D., Langen, P. L., Stevens, B., and Tomassini, L. (2013). Climate feedback efficiency and synergy. *Climate Dynamics*, 41:2539–2554.
40. Merlis, T. M. (2014). Interacting components of the top-of-atmosphere energy balance affect changes in regional surface temperature. *Geophysical Research Letters*, 41(20):7291–7297.
41. Merlis, T. M. and Henry, M. (2018). Simple estimates of polar amplification in moist diffusive energy balance models. *Journal of Climate*, 31(15):5811–5824.
42. Middlemas, E., Kay, J., Medeiros, B., and Maroon, E. (2020). Quantifying the influence of cloud radiative feedbacks on Arctic surface warming using cloud locking in an Earth system model. *Geophysical Research Letters*, 47(15):e2020GL089207.
43. Morrison, A., Kay, J. E., Frey, W., Chepfer, H., and Guzman, R. (2019). Cloud response to Arctic sea ice loss and implications for future feedback in the CESM1 climate model. *Journal of Geophysical Research: Atmospheres*, 124(2):1003–1020.
44. Mülmenstädt, J., Salzmann, M., Kay, J. E., Zelinka, M. D., Ma, P.-L., Nam, C., Kretzschmar, J., Hörnig, S., and Quaas, J. (2021). An underestimated negative cloud feedback from cloud lifetime changes. *Nature Climate Change*, 11(6):508–513.
45. Payne, A. E., Jansen, M. F., and Cronin, T. W. (2015). Conceptual model analysis of the influence of temperature feedbacks on polar amplification. *Geophysical Research Letters*, 42(21):9561–9570.
46. Pendergrass, A. G., Conley, A., and Vitt, F. M. (2018). Surface and top-of-atmosphere radiative feedback kernels for CESM-CAM5. *Earth System Science Data*, 10(1):317–324.
47. Pithan, F. and Mauritsen, T. (2014). Arctic amplification dominated by temperature feedbacks in contemporary climate models. *Nature Geoscience*, 7(3):181–184.
48. Polyakov, I. V., Alekseev, G. V., Bekryaev, R. V., Bhatt, U., Colony, R. L., Johnson, M. A., Karklin, V. P., Makshtas, A. P., Walsh, D., and Yulin, A. V. (2002). Observationally based assessment of polar amplification of global warming. *Geophysical Research Letters*, 29(18):25–1.
49. Previdi, M., Janoski, T. P., Chiodo, G., Smith, K. L., and Polvani, L. M. (2020). Arctic amplification: A rapid response to radiative forcing. *Geophysical Research Letters*, 47(17):e2020GL089933.
50. Roe, G. H., Feldl, N., Armour, K. C., Hwang, Y.-T., and Frierson, D. M. (2015). The remote impacts of climate feedbacks on regional climate predictability. *Nature Geoscience*, 8(2):135–139.
51. Russotto, R. D. and Ackerman, T. P. (2018). Energy transport, polar amplification, and ITCZ shifts in the GeoMIP G1 ensemble. *Atmospheric Chemistry and Physics*, 18(3):2287–2305.
52. Russotto, R. D. and Biasutti, M. (2020). Polar amplification as an inherent response of a circulating atmosphere: Results from the TRACMIP aquaplanets. *Geophysical Research Letters*, 47(6):e2019GL086771.
53. Schneider, T., Teixeira, J., Bretherton, C. S., Brient, F., Pressel, K. G., Schär, C., and Siebesma, A. P. (2017). Climate goals and computing the future of clouds. *Nature Climate Change*, 7(1):3–5.
54. Serreze, M., Barrett, A., Stroeve, J., Kindig, D., and Holland, M. (2009). The emergence of surface-based Arctic amplification. *The Cryosphere*, 3(1):11–19.
55. Shell, K. M., Kiehl, J. T., and Shields, C. A. (2008). Using the radiative kernel technique to calculate climate feedbacks in NCAR's Community Atmospheric Model. *Journal of Climate*, 21(10):2269–2282.
56. Siler, N., Roe, G. H., and Armour, K. C. (2018). Insights into the zonal-mean response of the hydrologic cycle to global warming from a diffusive energy balance model. *Journal of Climate*, 31(18):7481–7493.

57. Singh, H., Rasch, P., and Rose, B. (2017). Increased ocean heat convergence into the high latitudes with CO2 doubling enhances polar-amplified warming. *Geophysical Research Letters*, 44(20):10–583.
58. Smith, C., Kramer, R., Myhre, G., Forster, P., Soden, B., Andrews, T., Boucher, O., Faluvegi, G., Fläschner, D., Hodnebrog, Ø., et al. (2018). Understanding rapid adjustments to diverse forcing agents. *Geophysical Research Letters*, 45(21):12–023.
59. Smith, C. J., Kramer, R. J., Myhre, G., Alterskjær, K., Collins, W., Sima, A., Boucher, O., Dufresne, J.-L., Nabat, P., Michou, M., et al. (2020). Effective radiative forcing and adjustments in CMIP6 models. *Atmospheric Chemistry and Physics*, 20(16):9591–9618.
60. Soden, B. J. and Held, I. M. (2006). An assessment of climate feedbacks in coupled ocean–atmosphere models. *Journal of climate*, 19(14):3354–3360.
61. Soden, B. J., Held, I. M., Colman, R., Shell, K. M., Kiehl, J. T., and Shields, C. A. (2008). Quantifying climate feedbacks using radiative kernels. *Journal of Climate*, 21(14):3504–3520.
62. Stuecker, M. F., Bitz, C. M., Armour, K. C., Proistosescu, C., Kang, S. M., Xie, S.-P., Kim, D., McGregor, S., Zhang, W., Zhao, S., et al. (2018). Polar amplification dominated by local forcing and feedbacks. *Nature Climate Change*, 8(12):1076–1081.
63. Tan, I., Barahona, D., and Coopman, Q. (2022). Potential link between ice nucleation and climate model spread in Arctic amplification. *Geophysical Research Letters*, 49(4):e2021GL097373.
64. Tan, I., Sotiropoulou, G., Taylor, P. C., Zamora, L., and Wendisch, M. (2023). A Review of the Factors Influencing Arctic Mixed-Phase Clouds: Progress and Outlook. *Clouds and Their Climatic Impacts: Radiation, Circulation, and Precipitation*, pages 103–132.
65. Tan, I. and Storelvmo, T. (2019). Evidence of strong contributions from mixed-phase clouds to Arctic climate change. *Geophysical Research Letters*, 46(5):2894–2902.
66. Taylor, K., Crucifix, M., Braconnot, P., Hewitt, C., Doutriaux, C., Broccoli, A., Mitchell, J., and Webb, M. (2007). Estimating shortwave radiative forcing and response in climate models. *Journal of Climate*, 20(11):2530–2543.
67. Taylor, K. E., Stouffer, R. J., and Meehl, G. A. (2012). An overview of CMIP5 and the experiment design. *Bulletin of the American meteorological Society*, 93(4):485–498.
68. Vavrus, S. (2004). The impact of cloud feedbacks on Arctic climate under greenhouse forcing. *Journal of Climate*, 17(3):603–615.
69. Voigt, A., Albern, N., and Papavasileiou, G. (2019). The atmospheric pathway of the cloud-radiative impact on the circulation response to global warming: Important and uncertain. *Journal of Climate*, 32(10):3051–3067.
70. Wetherald, R. and Manabe, S. (1988). Cloud feedback processes in a general circulation model. *Journal of the Atmospheric Sciences*, 45(8):1397–1416.
71. Winton, M. (2006). Amplified Arctic climate change: What does surface albedo feedback have to do with it? *Geophysical Research Letters*, 33(3).
72. Zelinka, M. D., Myers, T. A., McCoy, D. T., Po-Chedley, S., Caldwell, P. M., Ceppi, P., Klein, S. A., and Taylor, K. E. (2020). Causes of higher climate sensitivity in CMIP6 models. *Geophysical Research Letters*, 47(1):e2019GL085782.
73. Zelinka, M. D., Randall, D. A., Webb, M. J., and Klein, S. A. (2017). Clearing clouds of uncertainty. *Nature Climate Change*, 7(10):674–678.